BERYLLIUM-BORON SYSTEMATICS OF ^{26}Al-POOR CAIs: IMPLICATIONS FOR THE RELATIONSHIP BETWEEN FUN AND NON-FUN CAIs. E.T. Dunham[1], M.-C. Liu[2], S.B. Simon[3], A.N. Krot[4], M. Wadhwa[1] [1]Center for Meteorite Studies, Arizona State University, Tempe, AZ 85287 (email: etdunham@asu.edu), [2]Dept. of Earth, Planetary, and Space Sciences, University of California, Los Angeles, CA 90095, [3]Institute of Meteoritics, University of New Mexico, Albuquerque NM 87131, [4]Hawai'i Institute of Geophysics and Planetology, University of Hawai'i at Manoa, Honolulu, HI 96822.

Introduction: Beryllium-10, which decays to ^{10}B with a half-life of 1.4 Ma, is produced almost exclusively by non-thermal nuclear reactions induced by solar energetic particles and galactic cosmic rays (e.g., [1]). It has been previously demonstrated that Ca-, Al-rich inclusions (CAIs) in several groups of carbonaceous chondrites record the prior existence of ^{10}Be. The inferred initial ^{10}Be/^{9}Be ratio, $(^{10}Be/^{9}Be)_0$, in CAIs with initial ^{26}Al/^{27}Al ratio, $(^{26}Al/^{27}Al)_0$, of ~5×10^{-5}, ranges from ~6×10^{-4} to ~10^{-2}, with most CAIs having a value of ~9×10^{-4} [2–9]. The few ^{26}Al-poor CAIs with FUN (i.e., Fractionation and Unidentified Nuclear) effects analyzed so far have lower $(^{10}Be/^{9}Be)_0$, ~3×10^{-4} [7].

Given the variability of the $(^{10}Be/^{9}Be)_0$ observed in different CAIs, it is important to consider the ^{10}Be-^{10}B system in the context of other isotopic systematics to better understand the origin of this variation. In particular, Δ^{17}O values in different phases of CAIs can provide insights into their alteration and transport histories [10]. In addition, the ^{26}Al-^{26}Mg system provides information about the age and thermal history of a CAI [1]. In this study, we report the $(^{10}Be/^{9}Be)_0$ of one FUN and one non-FUN CAI, which are characterized by low $(^{26}Al/^{27}Al)_0$, but different O-isotope compositions, to better understand their distinct formation environments.

Samples: FUN CAI *CMS-1* from the CV3.6 chondrite Allende is an igneous inclusion composed mainly of fassaite and melilite (~$Åk_{18–48}$) grains poikilitically enclosing abundant spinels. It is characterized by low $(^{26}Al/^{27}Al)_0$, large nucleosynthetic anomalies in Ti (ε^{50}Ti = -51.3±6.9), and mass-dependent fractionations in O, Mg, and Si isotopes [11]. Spinel is uniformly ^{16}O-rich (Δ^{17}O = -24.4±0.5‰); fassaite shows a range of Δ^{17}O (-24 to -14‰); melilite is uniformly ^{16}O-depleted (Δ^{17}O ~-3.5‰). On a three-isotope oxygen diagram, spinel compositions define a mass-dependent fractionation line with a slope of ~0.5, whereas fassaite and melilite plot along a line of slope ~1. Based on the chemical and isotopic compositions of *CMS-1* and high-temperature vacuum experiments, it is inferred that precursor of *CMS-1* was forsterite-rich and evaporated for only a few minutes in H_2-dominated gas at ~1900˚C [12].

CAI *31-2* from the CO3.0 chondrite Dominion Range (DOM) 08006 is an irregularly-shaped grossite-rich inclusion with a hibonite-grossite core surrounded by a multilayered rim sequence of melilite, Al-diopside, forsterite, and low-Ca pyroxene (Fig. 1). All minerals have ^{16}O-rich isotopic compositions with Δ^{17}O ranging from ~-25 to -20‰ [13]. It is characterized by a lack of mass-dependent fractionation in Mg and O isotopes, suggesting an insignificant role of evaporation during its formation. The CAI is mineralogically pristine, and shows no resolvable excess of radiogenic ^{26}Mg; the upper limit on the $(^{26}Al/^{27}Al)_0$ is $\leq4\times10^{-7}$ [13].

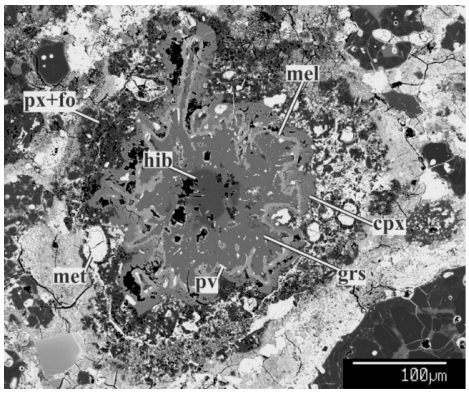

Fig. 1. BSE image of the CAI *31-2* from DOM 08006 (CO3.0). The CAI is composed of hibonite (hib), grossite (grs), perovskite (pv), melilite (mel), Fe,Ni-metal (met; oxidized) and is surrounded by layers of Al-diopside (cpx), forsterite (fo), and pyroxene (px).

Analytical Methods: Polished thin sections of *CMS-1* and *31-2* were thoroughly cleaned with mannitol to remove surface boron contamination. The B isotope compositions and Be/B ratios were measured with the UCLA Cameca IMS-1290 secondary ion mass spectrometer (SIMS) using an $^{16}O^-$ primary beam generated by a *Hyperion-II* source. The primary beam current of 10 nA resulted in a beam size ~5×4 μm^2. Secondary ion intensities were measured under mass resolving power of ~2,500 in dynamic multi-collection mode. In this setting, we first collected $^{27}Al^{3+}$ and $^{28}Si^{3+}$ simultaneously for 5 sec, then ^{9}Be for 10 sec after one mass jump, and then ^{10}B and ^{11}B for 30 sec as the last step. The NIST614 glass standard was measured throughout the analysis session to obtain the ^{9}Be/^{11}B relative sensitivity factor (RSF), and to correct for the instrumental mass fractionation on the ^{10}B/^{11}B ratio. Melilite-composition glasses with a range of

Be/B ratios were measured at the beginning of the session to verify that there were no resolvable matrix effects on the RSF [14]. Following these analyses, the SIMS spots on the CAIs were examined with the JEOL JXA-8520F electron microprobe at ASU; spots located on cracks were excluded from the isochron regression.

Results: We have previously reported the preliminary results of the Be-B analyses of *CMS-1*, showing small yet homogeneous excesses in the $^{10}B/^{11}B$ ratio relative to the chondritic value over a range of Be/B [14,15]. The data obtained here extend the range of Be/B and yield higher precision $^{10}B/^{11}B$ ratios, but still corroborate our previous results (weighted average $^{10}B/^{11}B = 0.251\pm0.002$). After combining all the data, we were only able to obtain an upper limit on the $(^{10}Be/^{9}Be)_0$ of $\leq4\times10^{-4}$, with an initial $^{10}B/^{11}B$ of 0.253±0.003. Figure 2 shows the Be-B isochron plot for CAI *31-2*. The data define a slope corresponding to a $(^{10}Be/^{9}Be)_0$ of $(1.5\pm0.7)\times10^{-3}$ (MSWD = 0.9) and an initial $^{10}B/^{11}B$ ratio of 0.245±0.002.

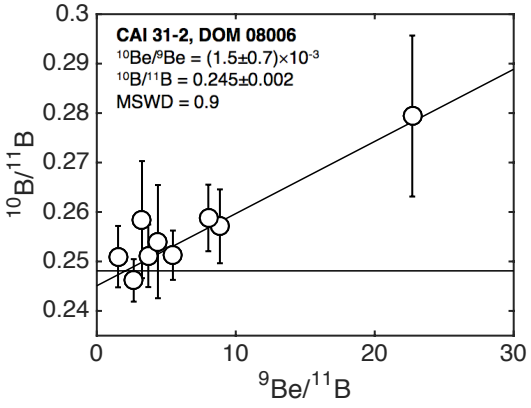

Fig. 2. The Be-B isochron for the CAI *31-2*. The horizontal line indicates the chondritic $^{10}B/^{11}B$ ratio [16]. Error bars are 2σ, based on counting statistics.

Discussion: The ^{26}Al-poor nature of the CAIs *CMS-1* and *31-2* suggests that they formed at a different time or place in the solar nebula than CAIs characterized by canonical $(^{26}Al/^{27}Al)_0$. Oxygen isotope compositions suggests that all phases in CAI *31-2* are relatively pristine and formed in an ^{16}O-rich reservoir [13]. In contrast, only the spinel grains in *CMS-1* preserve the isotopic signature of the ^{16}O-rich nebular reservoir from which this FUN CAI was originally formed, while melilite and fassaite have exchanged with other relatively ^{16}O-poor reservoirs that this CAI was subsequently exposed to [11]. The initial ^{10}Be abundances of these two inclusions provide additional insights into their formation environments and the subsequent thermal processing they may have encountered.

FUN CAI *CMS-1* likely originated as a forsterite-bearing inclusion, and subsequently underwent multiple heating events [11,12]. The lower concentration of Be in *CMS-1* compared to that in normal melilite-rich coarse-grained CAIs could be due to less Be being incorporated into the forsterite structure of the CMS-1 precursor. The homogeneous, yet elevated $^{10}B/^{11}B$ ratios (weighted average = 0.251±0.002, ~20‰ above the chondritic value) measured in *CMS-1* over a wide range of $^{9}Be/^{11}B$ suggest that ^{10}Be had been present in this CAI, but the inclusion was later equilibrated after this ^{10}Be had decayed away. The upper limit on the $(^{10}Be/^{9}Be)_0$ reported here ($\leq4\times10^{-4}$) is nevertheless consistent with the low value ($\sim3\times10^{-4}$) reported for other FUN CAIs. This value has been interpreted to be the background level of ^{10}Be inherited from the molecular cloud [7].

CAI *31-2*, on the other hand, was subjected to minimal (if any) secondary processing based on its O and Mg isotopic composition and its mineralogy [13]. The $(^{10}Be/^{9}Be)_0$ of $(1.5\pm0.7)\times10^{-3}$ in *31-2* is among the highest in ^{26}Al-poor inclusions studied so far, and is close to the typical $(^{10}Be/^{9}Be)_0$ in ^{26}Al-rich CAIs. Platy hibonite crystals (PLACs) in CM2 chondrites show isotopic features similar to those in *31-2*, including the large nucleosynthetic isotope anomalies and lack of ^{26}Al. However, the inferred $(^{10}Be/^{9}Be)_0$ of $(5\pm1)\times10^{-4}$ and elevated initial $^{10}B/^{11}B$ ratio (=0.2513) [6] in PLACs are resolvably different from those in *31-2*. This implies that while *31-2* and PLACs likely formed in a similar nebular environment, their irradiation histories (such as time or projectile flux) were distinct.

The inferred $(^{10}Be/^{9}Be)_0$ ratios in this study range from $\leq4\times10^{-4}$ to $(1.5\pm0.7)\times10^{-3}$. Although the low end of this range is consistent with the proposed background value of 3×10^{-4} [7], we argue that this and higher values are best understood in the context of *in situ* charged particle spallation. CAIs likely formed in a spatially-limited region very close to the Sun [1]. If the solar nebula inherited a baseline value of $^{10}Be/^{9}Be = 3\times10^{-4}$ from the molecular cloud, the ^{26}Al-poor inclusions, which could have formed in a common reservoir, should have been characterized by $(^{10}Be/^{9}Be)_0$ very close to this value, in contrast to our observation.

Acknowledgments: This work is supported by a NASA Earth and Space Science Fellowship (NNX16AP48H) to ED and a NASA Emerging Worlds grant (NNX15AH41G) to MW.

References: [1] Davis A.M. & McKeegan K.D. (2014), *Treatise on Geochemistry (2nd Ed.),* p.361. [2] McKeegan K.D. et al. (2000) *Science 289,* 1334. [3] Sugiura N. et al. (2001) *MAPS 36,* 1397. [4] MacPherson G.J. et al. (2003) *GCA 67,* 3165. [5] Chaussidon M. et al. (2006) *GCA 70,* 224. [6] Liu M.-C. et al. (2009) *GCA 73,* 5051. [7] Wielandt D. et al. (2012) *ApJ 748,* 25. [8] Gounelle M. et al. (2013) *ApJ 763,* 33. [9] Srinivasan G. et al. (2013) *EPSL 374*, 11. [10] Yurimoto H. et al. (2008) *Reviews M&G 68*, 141. [11] Williams C.D. et al. (2016) *GCA 201*, 25 [12] Mendybaev R.A. et al. (2016) *GCA 201*, 49. [13] Krot A.N. et al. (2017) *MetSoc,* Abstract #6056. [14] Dunham E.T. et al. (2017) *MetSoc,* Abstract #6381. [15] Dunham E.T. et al. (2017) *LPS 48,* Abstract #1507. [16] Zhai M. et al. (1996) *GCA 60*, 4877.